Bioactive Materials 22 (2023) 211–224

Contents lists available at ScienceDirect

Bioactive Materials

journal homepage: www.keaipublishing.com/en/journals/bioactive-materials

CD47KO/CRT dual-bioengineered cell membrane-coated nanovaccine combined with anti-PD-L1 antibody for boosting tumor immunotherapy

Shengyang Liu [a,b], Jiayan Wu [b], Yuanji Feng [b], Xiaoya Guo [b,c], Tong Li [b,c], Meng Meng [b,c], Jie Chen [b,**], Daquan Chen [a,***], Huayu Tian [b,c,*]

[a] School of Pharmacy, Key Laboratory of Molecular Pharmacology and Drug Evaluation (Yantai University), Ministry of Education, Collaborative Innovation Center of Advanced Drug Delivery System and Biotech Drugs in Universities of Shandong, Yantai University, Yantai, 264005, PR China
[b] Key Laboratory of Polymer Ecomaterials, Changchun Institute of Applied Chemistry, Chinese Academy of Sciences, Changchun, 130022, PR China
[c] College of Chemistry and Chemical Engineering, Xiamen University, Xiamen, 361005, PR China

ARTICLE INFO

Keywords:
CRISPR–Cas9
Dual-bioengineered cell membrane
Immune checkpoint blockade
Nanovaccine
Tumor immunotherapy

ABSTRACT

Tumor vaccines trigger tumor-specific immune responses to prevent or treat tumors by activating the hosts' immune systems, and therefore, these vaccines have potential clinical applications. However, the low immunogenicity of the tumor antigen itself and the low efficiency of the vaccine delivery system hinder the efficacy of tumor vaccines that cannot produce high-efficiency and long-lasting antitumor immune effects. Here, we constructed a nanovaccine by integrating CD47KO/CRT dual-bioengineered B16F10 cancer cell membranes and the unmethylated cytosine-phosphate-guanine (CpG) adjuvant. Hyperbranched PEI25k was used to load unmethylated cytosine-phosphate-guanine (CpG) through electrostatic adsorption to prepare PEI25k/CpG nanoparticles (PEI25k/CpG-NPs). CD47KO/CRT dual-bioengineered cells were obtained by CRISPR-Cas9 gene editing technology, followed by the cell surface translocation of calreticulin (CRT) to induce immunogenic cell death (ICD) in vitro. Finally, the extracted cell membranes were coextruded with PEI25k/CpG-NPs to construct the CD47KO/CRT dual-bioengineered cancer cell membrane-coated nanoparticles (DBE@CCNPs). DBE@CCNPs could promote endocytosis of antigens and adjuvants in murine bone marrow derived dendritic cells (BMDCs) and induce their maturation and antigen cross-presentation. To avoid immune checkpoint molecule-induced T cell dysfunction, the immune checkpoint inhibitor, the anti-PD-L1 antibody, was introduced to boost tumor immunotherapy through a combination with the DBE@CCNPs nanovaccine. This combination therapy strategy can significantly alleviate tumor growth and may open up a potential strategy for clinical tumor immunotherapy.

1. Introduction

Tumor vaccines can facilitate immune system recognition and elimination of tumor cells by inducing antitumor-specific immune responses. In recent years, a good progress has been made in clinical practice [1,2]. Scientists have identified many tumor-specific antigens (TSA) that are used to generate tumor vaccines [3,4]. However, personalized vaccines show unique advantages due to the diversity of tumor antigen epitopes between individuals [5]. Moreover, tumor cells often experience high mutation rates, which may result in the loss of one or more antigenic sites, and therefore, it is ideal to design vaccines that are directed against multiple epitopes [6]. A patient's autologous whole tumor cell antigen has the unique advantage of enabling dendritic cells to process and present a large number of tumor antigens, which triggers powerful polyclonal T cell responses to prevent tumor immune escape [7]. However, tumor cells evade immune surveillance by highly expressing immunosuppressive molecules that downregulate their immunogenicity [8,9]. Therefore, improving APCs' recognition and

Peer review under responsibility of KeAi Communications Co., Ltd.
* Corresponding author. Key Laboratory of Polymer Ecomaterials, Changchun Institute of Applied Chemistry, Chinese Academy of Sciences, Changchun, 130022, PR China.
** Corresponding author.
*** Corresponding author.
E-mail addresses: liushengyang0207@163.com (S. Liu), wujiayan@ciac.ac.cn (J. Wu), yjfeng@ciac.ac.cn (Y. Feng), xyguo12@ciac.ac.cn (X. Guo), tongli@ciac.ac.cn (T. Li), mmeng@ciac.ac.cn (M. Meng), chenjie@ciac.ac.cn (J. Chen), cdq1981@126.com (D. Chen), thy@xmu.edu.cn (H. Tian).

https://doi.org/10.1016/j.bioactmat.2022.09.017
Received 8 August 2022; Received in revised form 15 September 2022; Accepted 20 September 2022

uptake of whole tumor antigens is a key issue for its application as tumor vaccine.

CD47 is a transmembrane protein that is overexpressed on the surface of a variety of tumor cells. It can bind to signal-regulatory protein alpha (SIRPα) in myeloid cells and sends a "do not eat me" signal to avoid clearance by the immune system [10]. Blocking this pathway can promote the uptake of tumor cells by APCs, which is conducive to the presentation of tumor antigens [11]. Recently, researchers have developed CD47 antibodies that inhibit the CD47-SIRPα immune checkpoint pathway [12,13]. However, according to clinical data, CD47 antibodies may induce systemic side effects, including the accumulation or clearance of red blood cells [14]. Therefore, developing a safer and more efficient method to block CD47 is needed to improve the immunogenicity of tumor-associated antigens. However, blocking this signal alone cannot effectively promote the recognition of multiple antigens on the membrane surface by the immune system [15]. The main reason is the requirement of an "eat me" signal that guide antigen-presenting cells to perform phagocytosis. Preclinical studies have found that in addition to their original antitumor effects, chemotherapeutic drugs such as anthracyclines or taxanes, also induce the release of many immune stimulating signals by inducing immunogenic cell death (ICD) [16]. These signals can promote the endocytosis of tumor-associated antigens by phagocytes and stimulate the host to produce antitumor immune responses [17]. ICD typical biochemical characteristics are calreticulin (CRT) cell membrane translocation and the release of high mobility group box 1 (HMGB1) and adenosine triphosphate (ATP) [18,19]. It is particularly noteworthy that the translocated CRT can interact with its receptors on the surface of DCs and send "eat me" signals to promote antigen phagocytosis, which activates natural and adaptive immunity [20]. Thus, CD47 and CRT are a group of positive and negative signaling molecules that improves cell immunogenicity.

In addition, the inactivation of tumor infiltrating T cells is an important factor affecting the effect of immunotherapy [21]. Typically, tumor cells counteract immune cell clearance by upregulating PD-L1 expression [22,23], while also secreting exosomes to suppress naive T cell activation and effector T cell function [24,25]. Therefore, the commonly used strategy in combination therapy is the activation of tumor-specific effector T cells using tumor vaccines while also maintaining their antitumor capacity through an immune checkpoint blockade (ICB) strategy [26,27].

In this study, we designed a therapy strategy using a CD47KO/CRT dual-bioengineered cell membrane-coated nanovaccine combined with anti-PD-L1 antibody for boosting tumor immunotherapy. The CD47-SIRPα tumor phagocytosis checkpoint was knocked out in vitro using the CRISPR-Cas9 gene editing technology. The ICD of CD47 knockout tumor cells was induced by mitoxantrone in vitro. Then, cell membranes expressing "eat me" signals were extracted from these CD47KO/CRT dual-bioengineered tumor cells. The core of the nanovaccine was constructed by hyperbranched PEI25K that were loaded with unmethylated CpG adjuvant through electrostatic adsorption. CpG is an immunoadjuvant with a strong immunostimulatory ability that can be recognized by Toll-like receptor 9 (TLR9) in the APCs' endosomes [28]. The nanovaccine were prepared by coating CD47KO/CRT dual-bioengineered tumor cell membranes on immune adjuvant nanoparticles (PEI25k/CpG) by physical extrusion. The nanovaccine efficiently stimulated APCs, resulting in the stimulation of tumor-specific effector $CD8^+$ T cells which generate a powerful anti-tumor immune response. In melanoma mice, the nanovaccine was further used in combination with an immune checkpoint anti-PD-L1 antibody to further block the immunosuppressive effect of the tumor tissue on T cells. This

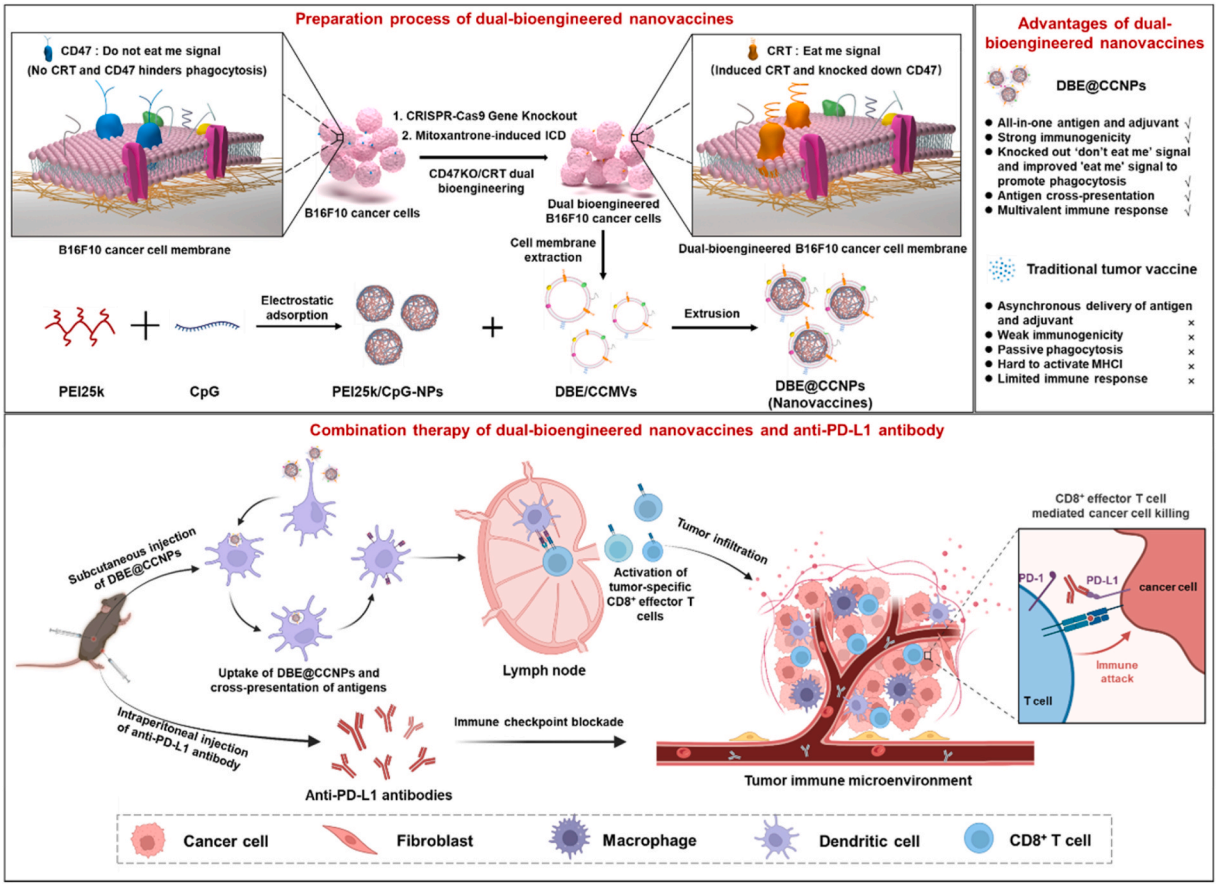

Scheme 1. Graphical figure showing the idea underlying the construction of the CD47KO/CRT dual-bioengineered cell membrane-coated nanovaccine and their anti-tumor therapeutic strategy in combination with an anti-PD-L1 antibody.

method led to satisfactory tumor suppression effects in tumor prevention and treatment models (Scheme 1). This study provides a personalized nanovaccine preparation platform technology through the bioengineering design of tumor cells, which can be used in combination with other therapeutic strategies as a potential strategy for clinical antitumor treatment.

2. Materials and methods

2.1. Materials

CpG oligodeoxynucleotide 1826 (5′-TCCATGACGTTCCTGACGTT-3′) and CpG-FAM were purchased from Sangon Biotech (Shanghai, China). The CRISPR/Cas9 targeting CD47 knockout plasmid is a pX458 vector encoding Cas9 and sgRNA for CD47 knockout (sgCD47-1: TTGGCGGCGGCGCTGTTGCT; sgCD47-2: ACTGCTGCGGCGCTGCTGGT) was ordered from GenePharma (Shanghai, China). Hyperbranched PEI (PEI25K, Mw 25,000 Da) was obtained from Sigma–Aldrich (St. Louis, USA). The Minute™ Plasma Membrane Protein Isolation and Cell Fractionation Kits were ordered from Invent Biotech (Beijing, China). NuPAGE 4x lithium dodecyl sulfate sample loading buffer (Novex) was purchased from Saixin Biotech (Changchun, China). Carboxyfluorescein diacetate, succinimidyl ester (CFDA SE), BeyoGel™ Plus PAGE Precast Gel (Hepes, 4–15%, 10-well), Lyso-Tracker Green, Lyso-Tracker Red and BCA Protein Assay Kit were obtained from Beyotime Biotech (Shanghai, China). Ultra HiFidelity PCR Kits and PCR Enhancer, TIANamp Genomic DNA Kit and TIANgel Purification Kit were ordered from Tiangen Biotech (Beijing, China). Ultrapure water (18 M.Q.cm) was obtained from the Millipore Milli-Q system. Mouse IL-12p40, calreticulin and IL-6 ELISA kits were ordered from Anoric Biotech (Tianjin, China). Sulfo-Cy5 NHS ester, Hoechst 33342 staining solution and mitoxantrone dihydrochloride were purchased from Meilun Biotech (Dalian, China). Details of all used antibodies are listed in Table S1. Recombinant murine granulocyte-macrophage colony stimulating factor (GM-CSF) and IL-4 were purchased from Peprotech (USA). GoldenTran-S transfection reagent was obtained from Golden Transfer Science and Technology Co.Ltd. (Changchun, China).

2.2. Cell lines and animals

Mouse B16F10 melanoma cells were obtained from Shanghai Cell Bank of the Chinese Academy of Sciences. The cells were cultured in Roswell Park Memorial Institute (RPMI) 1640 medium containing 10% fetal bovine serum at 37 °C in a 5% CO_2 atmosphere.

C57BL/6 mice (female, 6–8 weeks old) were purchased from Changsheng Experimental Animal Center (Benxi, China). All animal experiments complied with the relevant ethical standards and all procedures were approved by the Animal Care and Use Committee of Yantai University.

2.3. Construction and validation of CD47KO B16F10 cells

B16F10 cells (3×10^5 cells/plate) were seeded in 60 mm cell culture plates and cultivated overnight. A total of 20 μg of gene transfection reagent GoldenTran-S and 4 μg of CRISPR/Cas9-targeted CD47 gene knockout plasmid, were mixed and incubated for 10 min. When the cells were 70% confluent, the medium was replaced with serum-free medium and GoldenTran-S/pDNA nanoparticles were added. After incubation for 6 h, the serum-free medium was replaced by a medium containing 10% fetal bovine serum. After two days, the cells were digested with trypsin-EDTA (0.05%), stained with anti-mouse PE-CD47, and sorted by flow cytometry. CD47 knockout B16F10 cells (CD47KO-B16F10) were screened out through three rounds of cell sorting.

The successful knockout of CD47 was verified by gene sequencing. First, the total DNA of wild-type (WT) or CD47KO B16F10 cells was extracted with a TIANamp Genomic DNA Kit according to the manufacturer's instructions. PCR amplification experiments were performed using Ultra HiFidelity PCR Kits and PCR Enhancer according to the instructions. The primers' sequences used in this experiment were as follows: forward, 5′-GTCACGTCAACGAGCAGAGG-3'; reverse, 5′-CAGTTGCGGTTGTTCCCAGT-3'. Amplification conditions were as follows: Predenaturation at 94 °C for 120 s; 35 cycles of denaturation at 98 °C for 10 s; 60 °C for 30 s; 68 °C for 10 s; and extension at 68 °C for 300 s with a T100 thermal cycler (Bio–Rad, USA). Gene fragments of WT or CD47 knockout B16F10 cells were separated by agarose gel electrophoresis and recovered using a TIANgel Purification Kit. The concentration of DNA was determined by a MicroSpectrophotometer (KAIAO, Beijing). Two DNA fragments were sequenced at Comate Bioscience. (Changchun, China).

2.4. Induction and validation of ICD in vitro

WT or CD47KO B16F10 cells were cultured to induce ICD. For CRT induction, mitoxantrone dihydrochloride was added at a final concentration of 2 μM and incubated for 24 h. The collected cells were stained with Alexa Fluor® 488 anti-mouse CRT and detected by flow cytometry.

2.5. Endocytosis of different engineered cells in BMDCs

BMDCs were isolated from the tibias and femurs of C57BL/6 mice (female, 6–8 weeks old). Briefly, the tibias and femurs were dissected using tweezers and scissors, cleaned in 70% ethanol, and washed with PBS buffer. The bone marrow was flushed out with PBS buffer, pipetted into a single cell suspension, and passed through a 70-mesh sterile filter. The cells were centrifuged at 700×*g* for 8 min and resuspended in 10 mL of BMDCs growth media consisting of RPMI 1640 medium, 10% fetal bovine serum, 10 ng/mL GM-CSF, and 10 ng/mL interleukin-4 (IL-4). The cells were seeded in a dish at 2×10^5 cells/mL. After 24 h incubation, an additional 10 mL of BMDCs growth media was added, then half of the BMDCs growth media were changed every two days.

For the endocytosis assay, BMDCs were collected on day 7 and incubated in a 12-well plate at 1×10^5 cells per well. WT, CD47KO, CRT-induced, and CD47KO/CRT B16F10 tumor cells were labeled with CFDA SE according to the manufacturer's instructions and then co-cultured with BMDCs for 2 h at a ratio of 1:1 in a cell incubator. Nonspecific binding of BMDCs to tumor cells were tested at 4 °C. The cells were harvested and stained with a CD11C-APC antibody. Endocytosis was assessed by flow cytometry analysis of $APC^+CFDA\ SE^+$ double-positive cells. The phagocytosis index was obtained by dividing the value obtained at 37 °C by the value at 4 °C.

2.6. Preparation and characterization of different types of bioengineered cell membrane-coated PEI25k/CpG nanoparticles

PEI25k/CpG nanoparticles were obtained by electrostatic composite [29]. Briefly, CpG and hyperbranched PEI25k were dissolved in deionized water at concentrations of 0.1 μg/μL and 1 μg/μL, respectively. A total of 1 mL of CpG solution was pipetted into a tube, and then 50 μL of PEI25k solution was quickly dropped and immediately vortexed for 30 s. The encapsulation efficiency of CpG was detected via ultrafiltration and quantified by a nucleic acid protein tester.

The extraction method of tumor cell membrane fragments was performed as follows: The tumor cells were expanded in a cell culture dish (15 cm in diameter) and when cells reached 80–90% confluency, they were collected in PBS buffer by scraping and 1×10^7 cells were resuspended in 500 μL buffer A, which was supplemented with protease and phosphatase inhibitors. The cell suspension tube was incubated on ice for 8 min and vigorously vortexed for 20 s. Then, the cell suspension was immediately transferred to a filter cartridge and centrifuged at 16,000×*g* for 30 s. The pellet was resuspended by vigorous vortexing for 10 s. After centrifugation at 700×*g* for 60 s, the supernatant was transferred to a fresh tube and further centrifuged at 16,000×*g* for 30 min.

The pellet was further resuspended in 200 μL of buffer B. After centrifugation at 7800×*g* for 5 min at 4 °C, the supernatant was carefully transferred to a new tube and 1.6 mL of cold PBS buffer was added. The cell membranes' pellet was obtained after centrifugation at 16,000×*g* for 30 min and stored in deionized water at −80 °C. The concentrations of the extracted membrane proteins were determined using the BCA protein assay kit. The different bioengineered tumor cell membrane fragments used in this study were all extracted by this method.

The cancer cell membrane-coated PEI25k/CpG nanoparticles were prepared according to a previous extrusion approach [30,31]. Briefly, the cell membranes were extruded through a 400 nm polycarbonate membrane for 11 passes to form cancer cell membrane vesicles (CCMVs). Then, cancer cell membrane-coated nanoparticles (CCNPs) were prepared by mixing PEI25k/CpG-NPs with CCMVs and physically extruding through a 400 nm polycarbonate film for 11 passes using a mini-extruder.

The morphology of the nanoparticles was observed at 100 kV by a JEOL-1011 transmission electron microscope system (JEOL, Japan). Briefly, 10 μL CCNPs (0.5 mg/mL) was dropped into 400 square mesh copper grids with carbon support film. The droplets were dried with absorbent paper. The hydrate particle sizes and zeta potentials of the nanoparticles were detected using a zeta potential/BI-90 Plus particle size analyzer (Brookhaven, USA).

2.7. Gel electrophoresis experiment of PEI/CpG complex

Agarose gels at a 1% concentration, supplemented with Gel-Red, were prepared. Different ratios of the PEI/CpG complex were prepared, while keeping the mass of CpG always at 0.5 μg. A total of 10 μL of PEI/CpG complex was mixed with 2 μL of DNA loading buffer, then added to the agarose gel electrophoresis tank, and electrophoresed at 100 V for 30 min. Photographs were taken using a gel imaging equipment (Tanon 3500, Shanghai).

2.8. Cytotoxicity of the PEI/CpG complex

We evaluated the cytotoxicity of the PEI/CpG complex against BMDCs using the CCK8 assay. BMDCs were seeded in 96-well plates at a density of 1×10^4 cells per well and incubated for 24 h. After replacing with fresh medium, different concentrations of PEI/CpG complex were added to obtain the final concentrations of PEI at 0.5, 1.0, 1.5, 2.0, 2.5 μg/mL. After 24 h of incubation, 10 μL of the CCK8 solution was added to each well, and the incubation was continued for 1 h. The absorbance of the sample was measured at 450 nm using a microplate reader. The cell viability (%) was calculated according to the following formula: cell viability (%) = $(A_{sample}\text{-}A_{blank})/(A_{control}\text{-}A_{blank})$ x 100%.

2.9. Optimization of membrane coating

To explore the best mass ratio of cell membrane fragments and PEI25k/CpG nanoparticles, the membrane-coated nanoparticles were prepared by mixing 0.125–8 mg mass fragments of cell membranes and 1 mg of PEI25k/CpG nanoparticles. Membranes-free PEI25k/CpG nanoparticle cores were used as the control. The sizes of the nanoparticles were measured after preparation. Then, the same volume of 2 × PBS was added for 48 h at 37 °C. The stability of the membrane-coated nanoparticles was monitored. The smallest fluctuation in particle size was chosen to be the optimal membrane-to-core weight ratio.

2.10. Characterization of antigen retention of cell membrane vesicles and membrane-coated nanoparticles

The whole protein profile was characterized by SDS–PAGE. Briefly, the final protein concentration was quantified to be 2 mg mL^{-1} by the BCA method. Then, the samples were mixed with a loading buffer (Novex) and heated for 3 min at 100 °C. Then 20 μL of each sample was loaded into BeyoGel™ Plus PAGE Precast Gel (Hepes, 4–15%, 10-well) and proteins of different molecular weights were separated by electrophoresis at 150 V for 40 min. Finally, the gels were stained with Coomassie brilliant blue and imaged.

B16F10 tumor-specific antigens were evaluated by western blotting assay. Briefly, the proteins on the gel were transferred to a polyvinylidene fluoride (PVDF) membrane. Then, the membrane was blocked with 5% bovine serum albumin and incubated with primary antibodies against sodium potassium ATPase (Na^+/K^+-ATPase), Glycoprotein 100 (gp100) and Melanoma antigen recognized by T-cells 1 (MART1). The secondary anti-goat or anti-mouse IgG antibody was incubated with the corresponding primary antibodies prior to ECL imaging. The chemiluminescence of the substrate was imaged by a chemiluminescence imager (Amersham Imager 600, USA).

2.11. Colocalization of antigens and adjuvants

BMDCs were incubated overnight in confocal dishes at a density of 2×10^5 cells per well. The CD47KO/CRT membrane fragments were labeled with Sulfo-Cy5 NHS ester. Briefly, 20 μL of Sulfo-Cy5 NHS ester (1 μg/μL) was mixed with 100 μg of cancer cell membrane fragments. After 2 h, the cell membrane fragments were washed 3 times in PBS buffer and further coated onto the PEI25k/CpG nanoparticles. FAM-CpG was used in this study. The fluorescently labeled nanoparticles (10 μg/mL) were incubated in BMDCs for 2 h. Afterwards, the cells were washed 3 times with PBS buffer and then the cell nuclei were stained with Hoechst 33342 (0.01 mg/mL in PBS buffer) for 20 min. The prepared confocal dishes were observed using a confocal laser scanning microscope (CLSM) (ZEISS LSM780, Germany).

2.12. Endocytosis of four different membrane-coated nanoparticles by BMDCs in vitro

Four different cancer cell membranes (Normal/CCMVs, CRT/CCMVs, CD47KO/CCMVs, and DBE/CCMVs) were coated onto PEI25k/FAM-CpG nanoparticles. BMDCs were seeded into a 12-well plate at 1×10^5 cells/mL in BMDCs growth media. To evaluate the endocytosis efficiency, these membrane-coated nanoparticles were added and the final concentration of FAM-CpG was 1 μg/mL. Free FAM-CpG was used as the control. After incubation for 2 h, the cells were collected and analyzed by flow cytometry.

2.13. Activation of BMDCs by four different nanoparticles in vitro

Encouraged by the endocytosis effects of the four different membrane-coated nanoparticles in BMDCs, the activation of BMDCs was tested. Briefly, BMDCs were seeded into a 6-well plate at 2×10^5 cells per well and incubated with different nanoparticles for 2 h. The final concentrations of membrane and CpG were 5 μg/mL and 1.67 μg/mL, respectively. After 2 h incubation, the cells were washed twice and cultured for another 48 h. Afterwards, the supernatant was collected for IL-6 and IL-12p70 ELISA tests. BMDCs were washed 3 times, incubated with anti-CD11c-FITC, anti-MHC II-PE/Cy7, anti-CD80-APC and anti-CD86-PE antibodies at 4 °C for 45 min, washed 3 times with PBS buffer, and analyzed by flow cytometry.

2.14. Antitumor study of prophylactic vaccination

C57BL/6 mice (female, 6–8 weeks old) were randomly divided into 6 groups of 5 mice each. Different groups of mice were subcutaneously injected with PBS buffer, DBE/CCMVs, PEI25k/CpG-NPs, DBE/CCMVs + PEI25k/CpG-NPs, whole cell lysate (WC) +PEI25k/CpG-NPs, and DBE@CCNPs. The mice were immunized for three rounds with a one-week interval. Each group had 40 μg of tumor antigen and/or 20 μg of immune adjuvant. The tumor volumes and body weights of mice were measured every two days. The tumor volumes were calculated according

to the following formula: tumor volume (mm^3) = length × ($width^2$)/2. When the tumor volumes were greater than 1500 mm^3 (Day 20) in the PBS group, all the mice were euthanized.

2.15. Pharmacokinetics and biodistribution of components of nanovaccine

Cyanine 5.5 NHS ester was used to label the cell membranes, CpG, and PEI. The labeling method of the cell membranes was similar to that described in the above section 2.9. Cy5.5-CpG was purchased from Sangon Biotech. Cy5.5-PEI was obtained by mixing PEI with 2% Cy5.5 at room temperature and stirring for 6 h. DBE@CCNPs were prepared with the above Cy5.5 fluorescently labeled materials. The mice were divided into 3 groups and subcutaneously injected with DBE@CCNPs (Cy5.5-PEI), DBE@CCNPs (Cy5.5-membrane), and DBE@CCNPs (Cy5.5-CpG), respectively.

For the pharmacokinetics of nanovaccine, the blood of mice was collected at 0, 0.5, 1, 2, 4, 6, 12, 18, 24, 36, and 48 h into centrifuge tubes containing sodium heparin, and diluted 10 times with ultrapure water. The samples were transferred to 96-well black opaque plates, and the fluorescence intensity of blood was measured with a microplate reader (Tecan, Austria) at the excitation wavelength of 678 nm and emission wavelength of 694 nm.

For the biodistribution of the nanovaccine, in vivo fluorescence imaging was performed on the subcutaneous injection site of mice at 0, 6, 12, 24, 36, and 48 h, respectively. At 48 h, the heart, liver, spleen, lung, kidney, and lymph nodes were collected for fluorescence imaging.

2.16. Nanovaccine activates lymph nodes in vivo

To observe the ability of the nanovaccine to activate lymph node DCs in vivo, we sacrificed the mice 24 h after three immunizations and removed the mice draining lymph nodes for immunological analysis. The extracted tumor-draining lymph nodes were divided into a single cell suspension and cultured in a 24-well plate. After 48 h of culture, DCs and the supernatants were separated by centrifugation and analyzed for co-stimulatory molecules and cytokines, respectively. For analysis of DCs co-stimulatory molecules, the flow cytometry staining scheme of DCs is the same as that in section 2.13. For the analysis of DCs' secreted cytokines, their levels in the supernatants were monitored using IL-6 and IL-12p70 ELISA kits.

2.17. Endocytic pathway of DBE@CCNPs by BMDCs

BMDCs were pretreated with 10 μg/mL amiloride (AM), 5 μg/mL chlorpromazine (CPZ), and 4 μg/mL methyl-β-cyclodextrin (M-CD) at 37 °C for 45 min, respectively. DBE@CCNPs were prepared with FAM-labeled CpG. Then, DBE@CCNPs were added and incubated at 37 °C for 2 h. The control group was set up at 4 °C. The BMDCs were then pipetted down and washed 3 times with PBS buffer. The fluorescence intensity of BMDCs was analyzed using flow cytometry.

2.18. Observation of lysosomal escape of nanovaccine by CLSM

BMDCs were incubated overnight in confocal dishes at a density of 2×10^5 cells per well. Fam-CpG was used to prepare PEI25k/CpG-NPs and DBE@CCNPs. Cy5.5 NHS ester was used to label DBE/CCMVs. The materials were incubated with BMDCs for 1, 3, 8 h, respectively. The cells were then washed 3 times with PBS buffer. Lyso-tracker Red or Lyso-Tracker Green staining solution at 75 nM was added and incubated with BMDCs at 37 °C for 30 min. Samples were photographed by CLSM.

2.19. Prophylactic vaccination combined with anti-PD-L1 antibody therapy

C57BL/6 mice (female, 6–8 weeks old) were randomly divided into 4 groups of 5 mice each. The experimental groups were PBS control, DBE@CCNPs, α-PD-L1, and α-PD-L1 + DBE@CCNPs. The mice were immunized with DBE@CCNPs using 40 μg of cell membrane protein and 13.3 μg of CpG for 3 rounds and at an interval of one week each time. On the seventh day after the last immunization, 100 μL of B16F10 cells (5×10^6 cells/mL) were subcutaneously injected into the backs of the mice to generate subcutaneous tumors. On the 6th and 8th days after tumor inoculation, 30 μg of anti-PD-L1 antibody was intraperitoneally injected. The detailed experimental protocols were the same as mentioned above.

In survival experiments, mice were treated according to the immunization protocol described above, and mice were euthanized when the tumor size was greater than 1500 mm^3. The mice survival was observed until the 40th day.

2.20. Therapeutic vaccination combined with immune checkpoint therapy

C57BL/6 mice (female, 6–8 weeks old) were randomly divided into 4 groups with 5 mice in each group. On day 0, 100 μL of B16F10 cells (5×10^6 cells/mL) were subcutaneously injected into the backs of the mice to produce subcutaneous tumors. The subcutaneous injection of DBE@CCNPs (40 μg of cell membrane protein and 13.3 μg of CpG) was performed on day 5 and day 7. The PD-L1 antibody (30 μg) was intraperitoneally injected on day 6 and 8. The experimental groups and the experimental scheme were the same as mentioned above.

For immune cell analysis experiments, lymph nodes, spleen, and tumor tissues of mice were obtained and divided into single-cell suspensions in 12-well plates and filtered through 200-mesh cell strainers. The cells were collected by centrifugation and dispersed in 1.5 mL centrifuge tubes with 100 μL of PBS buffer. DCs in tumor-draining lymph nodes were stained using the previously mentioned staining protocol. The $CD8^+$ T cells ($CD3^+CD4^-CD8^+$) and the activated $CD8^+$ T cells ($CD3^+$ $CD8^+CD69^+$) in tumor, the $CD8^+$ T_{EM} cells ($CD3^+CD8^+CD44^+CD62L^-$) and the $CD8^+$ T_{CM} cells ($CD3^+CD8^+CD44^+CD62L^+$) in spleen were further evaluated.

2.21. Immunohistochemistry analyses

The infiltration of $CD8^+$ T cells and the expression of PD-L1 on tumor cells were detected by immunohistochemical experiments. Briefly, the prepared paraffin sections of tumor tissues were dried at 65 °C for 1 h, deparaffinized and rehydrated in xylene and graded alcohol (100%, 95%, and 75%). Antigen retrieval was performed using citrate buffer solution in accordance with the heat and pressure retrieval method. An incubation at 37 °C for 30 min with tenfold diluted serum was performed to block nonspecific sites. Then, the sample was cocultured with primary antibodies at 4 °C overnight. After co-incubating with the secondary antibodies, the Streptavidin-Biotin Complex (SABC) method was used for color development. Finally, hematoxylin was used for 2 min counterstaining. Immunohistochemistry (IHC) images were observed using an optical microscope (Nikon Y-TV55, Japan).

2.22. Safety evaluation

Hematoxylin and eosin (H&E) staining was used for pathological analysis of the main organs (heart, liver, spleen, lung, and kidney). In addition, the liver and kidney toxicities of the combination therapy were analyzed by blood biochemical indicators. The liver function was analyzed by detecting aspartate aminotransferase (AST), alanine aminotransferase (ALT), and alkaline phosphatase (ALP). The renal function was analyzed by creatinine (CRE), blood urea nitrogen (BUN), and uric acid (UA). These biochemical indicators were tested by ELSIA kits using an automatic microplate reader (Infinite M200, Tecan, Switzerland).

2.23. Statistics and data analysis

The Snapgene 2.3.2 software was used to analyze the gene

sequencing results. Flow cytometry results were performed using the FlowJov10 software. The statistical analysis was carried out using the unpaired two-tailed Student's *t*-test in the GraphPad Prism 8.0 Software.

3. Results

3.1. Construction and verification of the dual-bioengineered B16F10 tumor cells

Eliminating the "do not eat me" signals [11] or increasing the "eat me" signals [20] on tumor cells can activate immune cells and promote the hosts' antitumor immune killing effect. Based on this, we constructed a CD47KO/CRT dual-bioengineered cell membrane-coated nanovaccine.

First, the CD47 protein on the surface of B16F10 cells, which can assist tumor cells escape the uptake of antigen-presenting cells, and thus, avoid immune surveillance, was knocked out using the CRISPR–Cas9 gene editing technology. This signal blocking method does not involve the use of an CD47 antibody, thus avoiding toxicity to blood cells. Gene editing was performed under the action of a CRISPR/Cas9-targeted CD47 gene knockout plasmid, and the CD47-deficient B16F10 cell line was obtained after 3 cycles of cell sorting. The gene knockout efficiency was verified by gene sequencing. The results showed that the gene sequence had an uncertain set of nested peaks compared with the genome of wild-type B16F10 cells at the designed knockout site (Fig. 1a). This was mainly due to the nonhomologous end joining (NHEJ) repair of the genome in tumor cells, which caused the deletion of a part of the gene sequence or the insertion of a part of the gene fragment. CD47 knockout was further confirmed by flow cytometry (Fig. 1b).

In addition, to eliminate the "do not eat me" signal, the addition of a "eat me" signal is also very important to improve the immunogenicity of the antigen [15]. Typically, when the tumors exhibit ICD, tumor cells change from nonimmunogenic to highly immunogenic. This process was accompanied by changes in the expression levels of several signaling molecules on the cell membrane surface and the release of immune-promoting effectors [19]. However, some factors could also shift the tumor immune microenvironment from an immune-promoting type to an immunosuppressive type after ICD induction [32,33]. This is due to the release of a large amount of ATP in the process of ICD in tumor tissue, which is further metabolized into adenosine (ADO) by an exonuclease [34]. ADO is an immunosuppressive metabolite that can bind to ADO 2A receptors on the surface of immune cells [35]. It can limit the activation of cytotoxic lymphocytes and inhibit the maturation of natural killer cells, thereby impairing the antitumor immune response [33]. Moreover, in tumor cells' late ICD stage, the cells rupture and release potassium ions into the extracellular space [32]. Under normal circumstances, potassium ions are present in high concentrations inside the cell rather than outside the cell. The increased levels of potassium ions can reduce the activity and antitumor effect of T cells [36]. Therefore, to avoid these problems, we induced tumor cells' ICD in vitro and applied it in vivo after calreticulin translocation. Mitoxantrone is commonly used anthracycline in clinic that can induce tumor cell apoptosis cause ICD [16]. To maximize the translocation of CRT to cell membranes, we optimized the drug concentration and incubation time on that of calreticulin induction. Flow cytometry results demonstrated that the expression of calreticulin achieved the maximum value at 2 μM of Mitoxantrone after 24 h incubation, indicating a high translocation of calreticulin in tumor cells (Fig. S1). The exposure of calreticulin was further confirmed by flow cytometry assay (Fig. 1c). Furthermore, the cell membranes were extracted for calreticulin quantification by ELISA and the results achieved the same trends (Fig. S2).

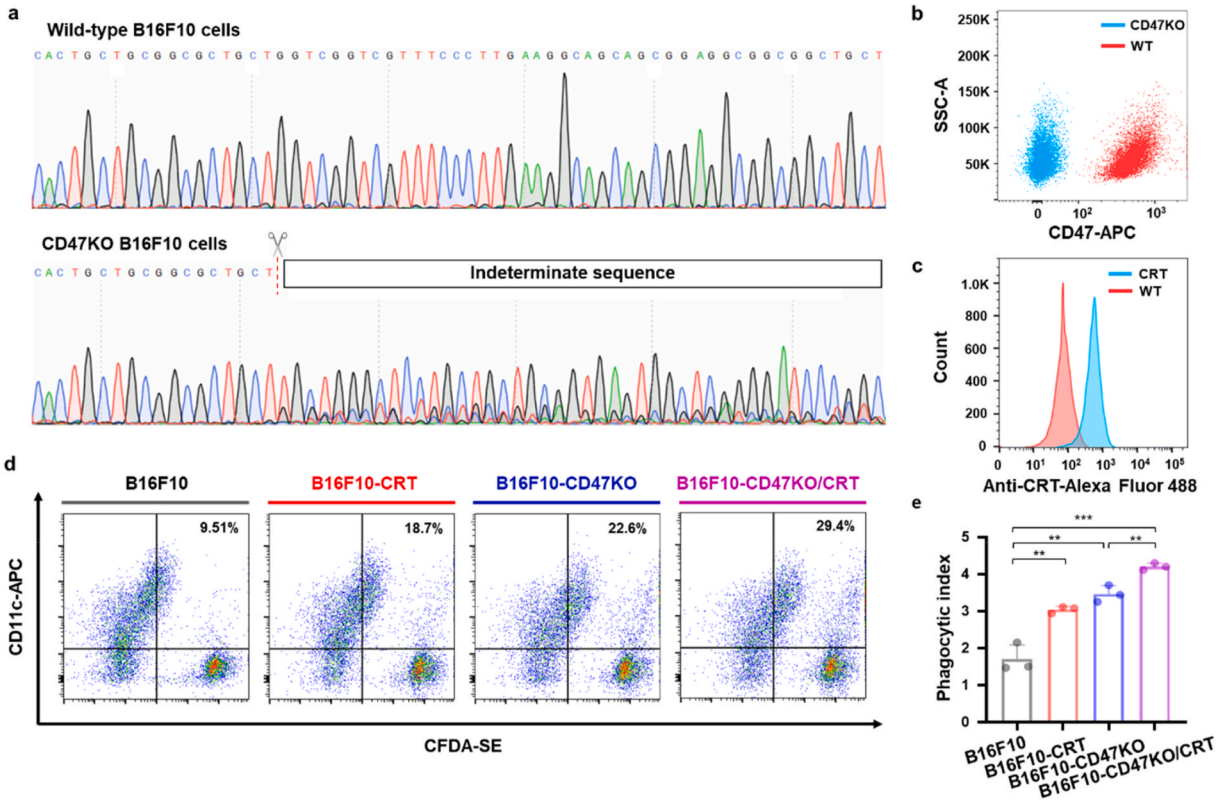

Fig. 1. Validation and functional exploration of dual-bioengineered B16F10 tumor cells. (a) Gene sequencing results of wild-type (WT) and CD47KO B16F10 cells. (b) Flow cytometry results of CD47 expression on WT and CD47KO B16F10 cells. (c) CRT translocation after induction of ICD under optimal conditions. (d) Phagocytosis of different bioengineered tumor cells by BMDCs. (e) The phagocytosis index was obtained by dividing the obtained value at 37 °C and that at 4 °C (n = 3). **p < 0.01, ***p < 0.001.

Encouraged by the success of CD47KO/CRT dual-bioengineered cells, we next evaluated the endocytosis efficiency of the prepared bioengineered B16F10 tumor cells in BMDCs. The results demonstrated that the endocytosis effects of B16F10-CRT and B16F10-CD47KO cells are significantly improved in BMDCs, while CD47KO/CRT dual-bioengineered cells achieved the optimal endocytosis effect (Fig. 1d and e). This might be due to that knocking out of CD47 protein alone could only eliminate the "do not eat me" signal between tumor cells and immune cells, while there was still a lack of a "eat me" signal to promote BMDCs phagocytosis. Therefore, when CRT translocated to the cells' membrane surface, it conferred an "eat me" signal to the cells, which further promoted the phagocytosis of BMDCs.

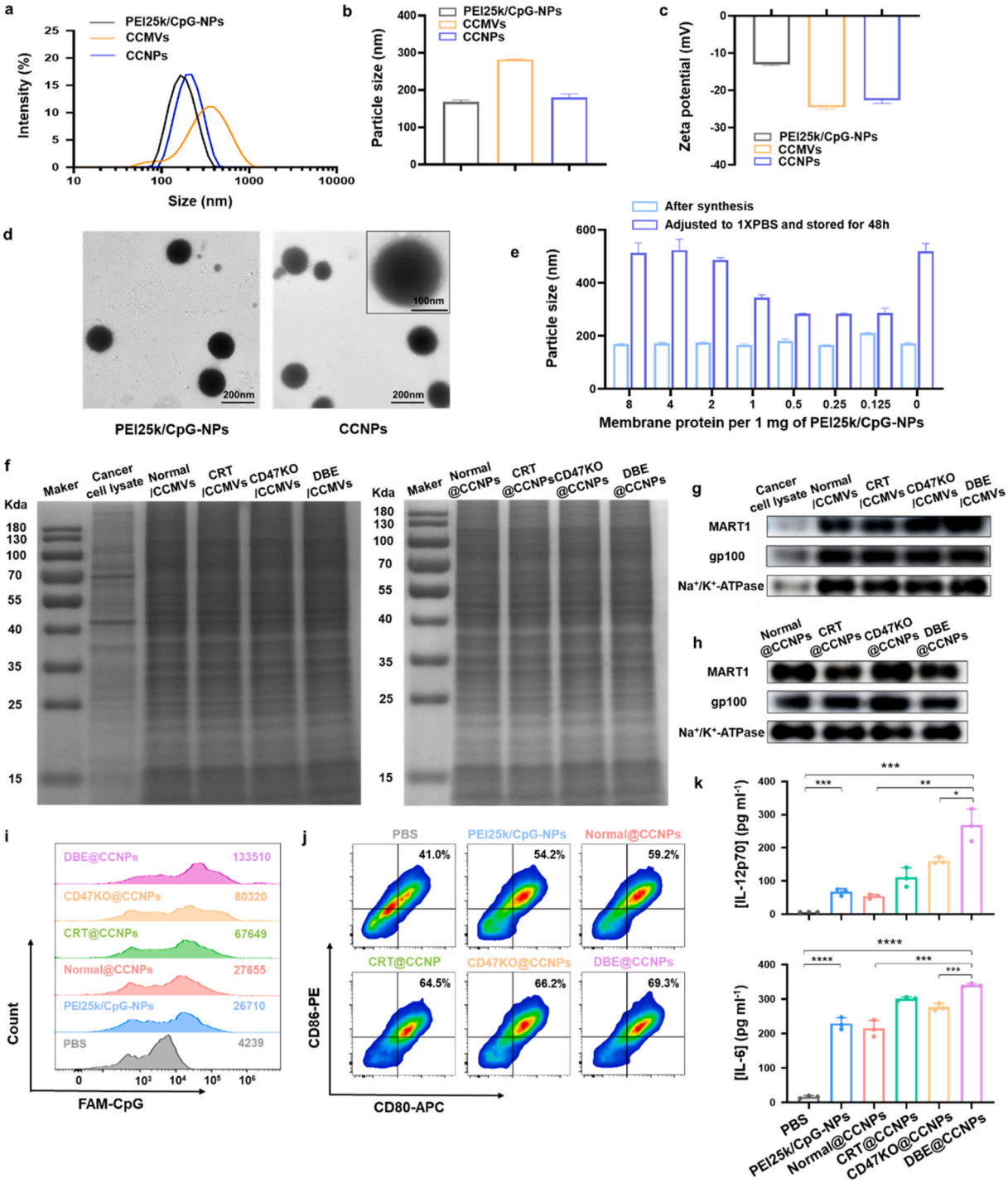

Fig. 2. Physicochemical identification and biofunctional verification of DBE@CCNPs. (a) Size intensity curves of PEI25K/CpG-NPs, CCMVs, and CCNPs. (b) Hydrodynamic size of PEI25K/CpG-NPs, CCMVs and CCNPs (n = 3). (c) Zeta potentials of PEI25K/CpG-NPs, CCMVs and CCNPs (n = 3). (d) TEM of PEI25k/CpG-NPs and CCNPs. (e) Hydrodynamic size of CCNPs at different mass ratios of membrane protein to PEI25k/CpG-NPs, right after synthesis, and after mixing with 2 × PBS and storage for 48 h (n = 3). (f) SDS-PAGE protein analysis of cancer cell lysates, different types of bioengineered CCMVs and CCNPs. (g–h) Western blotting analysis for membrane-specific proteins, including MART1, gp100, and Na^+/K^+-ATPase. (i) Endocytosis efficiency of the different types of bioengineered CCNPs by BMDCs. (j) Representative flow cytometry data showing that different types of bioengineered CCNPs can induce DCs maturation. (k) Secretion of IL-6 and IL-12p70 after endocytosis of the different types of nanoparticles. ****P < 0.0001; ***P < 0.001; **P < 0.01; *P < 0.05.

3.2. Preparation and characterization of the dual-bioengineered B16F10 tumor cell membrane-coated nanoparticles

The cell membranes of single/dual-bioengineered B16F10 tumor cells were extracted as the antigen of tumor vaccines' antigens. Since the translocation of calreticulin and the CD47 knockout occurred on tumor cell membranes, extracting the cell membrane as antigens could not only inherit the broad antigen spectrum and bioengineering characteristics of tumor cells, but also remove the huge cellular organelle structure, thereby paving the way for the subsequent preparation of a tumor nanovaccine [37]. The cell lysates were harvested by repeated freezing and thawing to completely rupture the tumor cells and the cell plasma membranes were separated from other cell components by centrifugation. Afterwards, the cytoplasmic membranes were extruded into vesicles through a 400 nm porous polycarbonate membrane. The hydrated particle size of the vesicles was approximately 283 nm, and the zeta potentials were −24 mV. (Fig. 2a and b).

The delivery strategy of tumor antigens is also crucial to the final immune effect [38,39]. Nanodelivery systems have been widely used in the field of vaccines due to their unique advantages. These include codelivery of antigens and immune adjuvants, enhancing the uptake of APCs, and improving the materials' biological distribution [40,41]. Therefore, we mixed hyperbranched PEI25k with immune adjuvant CpG to construct the nanodelivery carrier by electrostatic adsorption. The uniform nanoparticles were obtained with a hydrodynamic diameter of 165 nm. (Fig. 2a). The zeta potentials of PEI25k/CpG nanoparticles were −13 mV (Fig. 2b), which was convenient for their encapsulation by cell membranes. To confirm that CpG was completely integrated into the PEI/CpG complex, we performed DNA gel electrophoresis experiments. The experimental results showed that CpG was completely blocked when the PEI was 0.5 times that of CpG (Fig. S3). To evaluate the biocompatibility of this nanocomposite, we characterized the cytotoxicity of PEI/CpG using the CCK-8 assay. The results showed that the toxicity of PEI/CpG complex is negligible (Fig. S4). This is because only a small amount of PEI is required to adsorb CpG to form nanoparticles. However, in gene transfection experiments, the mass of PEI is often ten times that of the plasmid [42,43]. As a result, the excessive use of PEI resulted in cytotoxicity. However, the PEI in our nanovaccine is one-half the mass of CpG. Thus, the dose of the used PEI in this study was within the safe range and did not cause cytotoxicity.

To simultaneously deliver antigens and adjuvants and exert a spatiotemporal synergistic effect, we constructed cell membrane-coated nanoparticles by coextruding cell membrane vesicles with PEI25k/CpG-NPs cores. The final hydrodynamic diameters of cell membrane-coated nanoparticles increased to approximately 184 nm and their zeta potentials decreased to −22 mV (Fig. 2a, b and c). The increased particle size was about 20 nm, which was equivalent to the thickness of the two cell membranes, and the final zeta potentials also appeared to be consistent with the zeta potential of the membrane vesicles. TEM images of the nanoparticles also showed a clear core-shell structure (Fig. 2d). The outermost cell membrane structure was clearly visible. These results indicated the successful construction of cell membrane-coated nanoparticles. To optimize the efficiency of the cell membranes' encapsulation, we evaluated the optimal composite ratio of PEI25k/CpG nanoparticles and the cell membranes through stability experiments. As shown in Fig. S5, the particle size of bare nanoparticles was extremely unstable and increased rapidly in PBS solution. However, the particle size of CCNPs did not change significantly in PBS solution, which was mainly due to the shielding of ion interference in PBS solution by the coated cell membrane. As shown in Fig. 2e, the hydrodynamic particle sizes of the membrane-coated nanoparticles show that their best stability is achieved at their mass ratio of 2:1. It is worth noting that excessive cell membrane does not increase the stability of nanoparticles. This may be due to the fact that excessive cell membrane may affect the integrity of cell membrane which coated on the surface of nanoparticles during the process of co-extrusion preparation of nanoparticles.

After optimizing the ratio of membrane protein to nanoparticle core, we further verified the integrity of the membrane surface functional proteins after assembly of the nanovaccine by SDS–PAGE and Western blot experiments. SDS–PAGE results showed that the protein profile of the membrane-coated nanoparticles closely matched that of the corresponding membrane vesicles (Fig. 2f), demonstrating the integrity of the membrane proteins during the nanovaccine preparation. Furthermore, the Western blot results confirmed that the specific antigens gp100 and MART1 of B16F10 tumor cells and Na^+/K^+-ATPase in the cell membranes, were not damaged during the nanovaccine preparation (Fig. 2g and h). The different grayscale in WB bands indicated the degree of antigen enrichment in the nanoparticles, which was much greater than that in pure tumor cell lysates. These results suggested that the efficiency of cell membrane antigens was higher than that of tumor cells or pure tumor cell lysates under the same protein condition.

To verify whether the membrane-coated nanovaccine could simultaneously and successfully deliver the antigens and adjuvants into BMDCs, we used Cy5-HNS labeled cell membranes and FAM-CpG to construct a nanovaccine and evaluated its intracellular uptake in BMDCs. CLSM images showed that the red fluorescence and green fluorescence signals colocalize, indicating that the membrane-coated nanoparticles can spatiotemporally co-deliver antigens and immune adjuvants so that the two components can play a synergistic effect (Fig. S6). In addition, we detected the endocytosis efficiency of different bioengineered cell membranes-coated nanovaccine in BMDCs. Fluorescence quantitative results showed that the uptake of BMDCs in the dual-bioengineered B16F10 cancer cell membrane-coated nanoparticles (DBE@CCNPs) was significantly higher than that of the CD47KO B16F10 cancer cell membrane-coated nanoparticles (CD47KO@CCNPs) or CRT-induced B16F10 cancer cell membrane-coated nanoparticles (CRT@CCNPs) (Fig. 2i). This further proved that DBE@CCNPs inherited the biological functions of the cell membrane and promoted the endocytosis of the nanovaccine in APCs.

Then, we evaluated the maturation of BMDCs induced by different types of bioengineered cell membrane-coated nanovaccine in vitro. The expressions of costimulatory markers on BMDCs were detected by flow cytometry. The secretion of the immune factors, IL-6 and IL-12P70, by BMDCs were tested by ELISA. Compared with the PBS group, the PEI25k/CpG nanoparticles (PEI25k/CpG-NPs) treated group showed a significant upregulation of costimulatory molecules (Fig. 2j) and the secretion of immune factors (Fig. 2k), indicating that the immune adjuvant nanoparticle core could induce the maturation of BMDCs. For the group of nanoparticles coated with different types of bioengineered cell membranes, they can all activate the maturation of BMDCs, but the mechanism of activating the maturation of BMDCs is different. For the CD47KO@CCNPs group, knockout of CD47 can remove the "don't eat me" signal and increase the phagocytic efficiency of BMDCs to nanoparticles. For the CRT@CCNPs group, CRT can bind to low-density lipoprotein receptor related proteins on the surface of BMDCs, thereby enhancing the activation of BMDCs and improving the phagocytic efficiency of BMDCs to nanoparticles [44]. We noticed that the stimulation effect of DBE@CCNPs group on BMDCs was significantly better than those of the single bioengineered CCNPs group or the non-bioengineered CCNPs group. This was due to the two signals on the cell membrane cooperate with each other, so that the nanovaccine could efficiently induce the maturation of BMDCs (Fig. 2j and k).

3.3. Antitumor immunotherapy of the tumor nanovaccine

We have proved that dual-bioengineering technology can significantly improve the immunogenicity of tumor antigens in vitro. Next, we evaluated the antitumor efficiency of different assembly forms of adjuvant and antigen to optimize in vivo conditions. First, we subcutaneously injected different types of materials into mice, including dual-bioengineered cancer cell membrane vesicles (DBE/CCMVs), PEI25k/CpG-NPs, vortex mixing of double bioengineered whole cell lysate and

PEI25k/CpG-NPs (DBE/WC + PEI/CpG-NPs), vortex mixing of DBE/CCMVs and PEI25k/CpG-NPs (DBE/CCMVs + PEI/CpG-NPs), and coextrusion mixing of DBE/CCMVs and PEI25k/CpG-NPs (DBE@CCNPs). To achieve a long-term immune memory effect, we adopted a preventive tumor vaccine immunization strategy, with a total of 3 immunization rounds, each with a one-week interval (Fig. 3a). On day 0, B16F10 tumor cells were subcutaneously injected to the mice and the growth curves of the tumors were monitored. The results showed that the therapeutic effect of PEI25k/CpG-NPs was comparable with that of the PBS control group, due to the absence of antigens. The immune adjuvant alone could hardly trigger a specific antitumor immune response (Fig. 3b and c and S7). DBE/CCMVs showed a limited therapeutic effect. This suggested that multiple antigen vaccinations can achieve a certain immune effect, but not enough to inhibit the rapid growth of tumors. In addition, the DBE/WC + PEI/CpG-NPs and DBE/CCMVs + PEI25k/CpG-NPs groups slowed down the growth rate of tumors, and their preventive effects were not significantly different. The best tumor prevention effect was observed in the DBE@CCNPs group, and the preventive effect was around 75% compared with that in the PBS group (Fig. 3c).

To evaluate the anti-tumor mechanism of the tumor nanovaccine, we tested the physical behavior of the nanovaccine and the activation of the

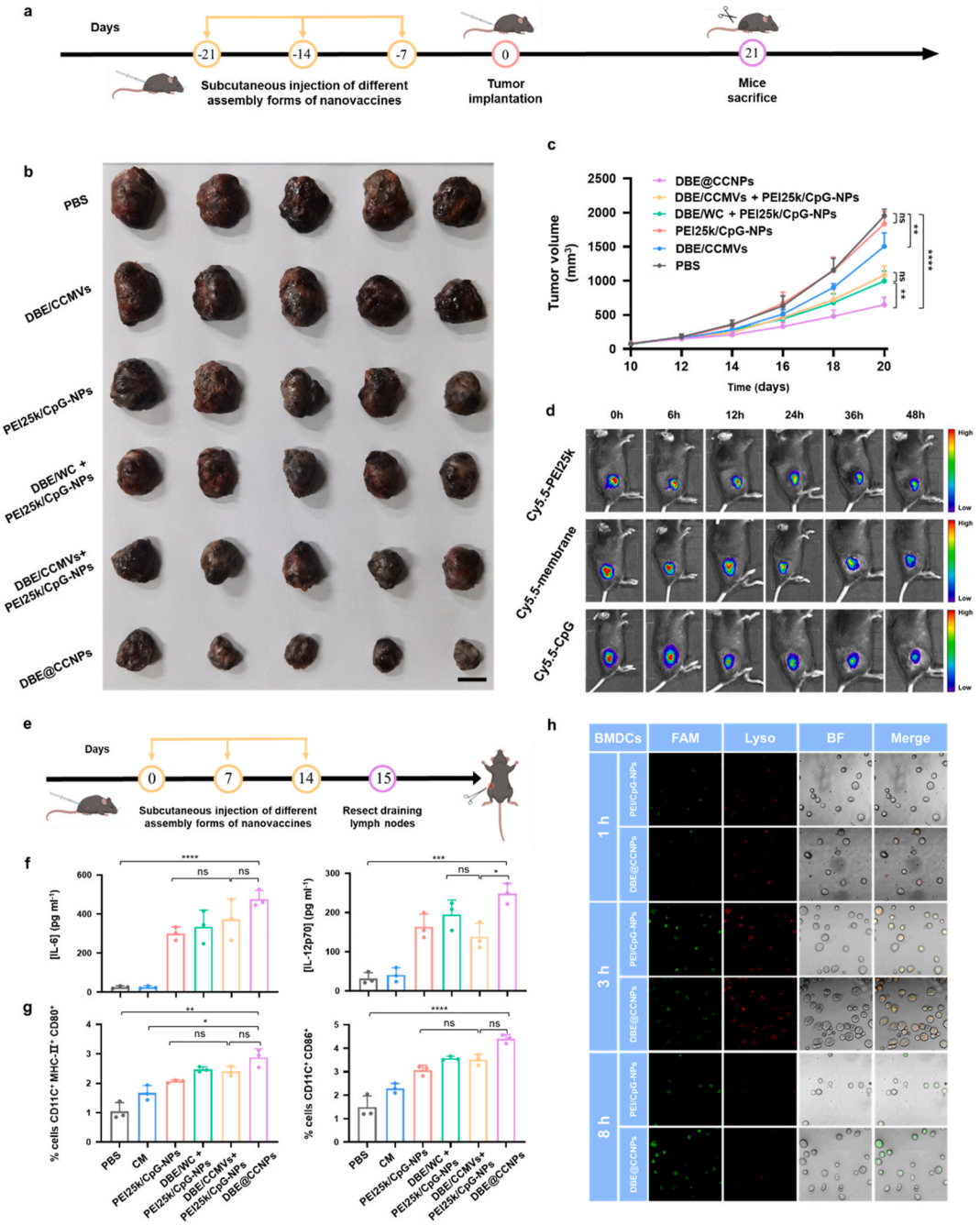

Fig. 3. The prophylactic efficacy of different assembly forms of tumor nanovaccine. (a) Schematic strategy for antitumor study. (b) Photos of the tumors after treatment. Scale bar = 1 cm. (c) Tumor growth curves of different groups. (d) Fluorescence imaging of the nanomaterials at the administration sites over time and after subcutaneous injection. (e) Treatment scheme for detecting the activation of the antigen-presenting cells by the nanovaccine. (f) Concentrations of proinflammatory cytokines in lymph nodes, including IL-12p70 and IL-6. (g) DC maturation in the lymph nodes. (h) The lysosomal escape behaviors of PEI/CpG-NPs and DBE@CCNPs in BMDCs were observed by confocal laser microscopy. Scale bar = 50 μm ****$p < 0.0001$; ***$p < 0.001$; **$p < 0.01$; *$P < 0.05$; ns, not significant.

antitumor immune response in vivo. We first tested the residence ability of the nanovaccine at the subcutaneous injection site. The results of in vivo fluorescence imaging of the mice showed that there was still a strong fluorescence at 48 h, indicating that the nanovaccine can form a subcutaneous tumor vaccine repository and activate APCs for a long time (Fig. 3d and S8). In addition, the experimental results of the nanovaccine biological distribution showed that the nanomaterials mainly accumulate in lymph nodes, and that the main components are metabolized through the liver and kidney pathways (Fig. S9). Next, we explored the activation of the immune system by the nanovaccine. On the second day after the 3 immunization rounds, the lymph nodes of the mice were resected for the analysis of DCs' activation and the secretion of cytokines (Fig. 3e). Data on the costimulatory molecule expression and secretion of cytokines showed that the DBE/CCMVs + PEI25k/CpG-NPs group is not as effective as the DBE@CCNPs group in DCs' activation, but it was approximatively equivalent to that of pure adjuvant nanoparticles (Fig. 3f and g). These results suggested that DCs' activation was mainly due to the uptake of immune adjuvants, and that the dual-bioengineered membranes can improve the endocytosis efficiency of the immune adjuvant nanoparticles. However, the DBE/CCMVs + PEI25k/CpG-NPs group can only deliver antigens and adjuvants separately, leading to a poor DCs' activation. Therefore, we used the coextrusion mixing method as the preparation form of the tumor nanovaccine.

We also explored the interaction between the nanovaccine and DCs. We first explored DBE@CCNPs pathway of endocytosis by DCs. The experimental results showed that the endocytosis efficiency of DBE@CCNPs at 4 °C was significantly lower than that at 37 °C (Fig. S10). This indicates that the endocytic behavior of DBE@CCNPs by BMDCs is energy dependent. Next, we found that in the group pretreated with M-CD, the endocytosis efficiency of DBE@CCNPs decreases to 40% of the original, indicating that the endocytosis of DBE@CCNPs is a caveolae-mediated endocytic pathway. Then, we carried out lysosomal escape experiment of the nanovaccine. DCs' antigen cross presentation requires the escape of the tumor antigen to from the lysosomes, otherwise it cannot trigger a $CD8^+$ anti-tumor immune response [45]. Therefore, it was particularly critical to explore whether the nanovaccine can perform a lysosomal escape. For this, we used the Lyso-Tracker Red to stain lysosomes and the FAM to label nanoparticles to study the lysosomal escape behavior of DBE@CCNPs in BMDCs. As shown in Fig. 3h, PEI/CpG-NPs and DBE@CCNPs were incubated with BMDCs for 1 h, 3 h and 8 h, respectively. A yellow fluorescence indicates the overlap of nanoparticles with lysosomes. At 1 h, we observed a small amount of yellow area in the BMDCs, indicating that the nanoparticles began to enter the BMDCs. At 3 h, a large yellow area was observed, indicating that more nanoparticles were endocytosed by the BMDCs and entered the lysosomes. It is worth noting that at 8 h, we observed an obvious green fluorescence, while the red fluorescence became significantly darker. This is due to breakdown of the lysosomes. The results indicated that the nanoparticles escaped from the lysosomes. However, the lysosomal escape did not occur in the DBE/CCMVs group at 8 h (Fig. S11). This suggests that the lysosomal escape ability of DBE@CCNPs is endowed by internal PEI/CpG-NPs. This may be attributed to the "proton sponge" effect of the PEI lipid [46].

3.4. Prophylactic nanovaccine combined with anti-PD-L1 antibody for antitumor immunotherapy

PD-L1 is overexpressed on the surface of tumor cells where it binds to T cells PD-1 to impair their antitumor effects [47,48]. Normally, tumor cells are capable of upregulating the expression levels of PD-L1 to combat the continuous infiltration of T cells [49]. At the end of the previous tumor suppression experiment, we immunohistochemically detected PD-L1 expression on tumors in the PBS and DBE@CCNPs groups. As shown in Fig. S12, the immunohistochemical results of PD-L1 on tumor tissues also proved that the tumor nanovaccine alone can induce the upregulation of PD-L1 expression. Therefore, an anti-PD-L1 antibody was introduced to boost the antitumor effect of the DBE@CCNPs nanovaccine.

The detailed combined antitumor immunotherapy was performed as shown in Fig. 4a. The tumor sizes were monitored every two days (Fig. 4b and S13). The results showed that compared with the vaccine or anti-PD-L1 antibody group, the combined group significantly delayed tumor growth (Fig. 4c and d). Blocking PD-1/PD-L1 immune checkpoint could effectively boost the antitumor immune effect of the DBE@CCNPs nanovaccine. We also conducted survival experiments on mice, and the results demonstrated that the survival time of mice in the combination treatment group was significantly prolonged (Fig. S14).

3.5. Therapeutic nanovaccine combined with anti-PD-L1 antibody for antitumor immunotherapy

The strategy of the combined application of a therapeutic nanovaccine and anti-PD-L1 antibody is shown in Fig. 4e. The mice were subcutaneously immunized twice on day 5 and day 7. Anti-PD-L1 antibody was intraperitoneally injected on day 6 and day 8. All mice were euthanized when the tumors' size in the PBS group was greater than 1500 mm^3. Lymph nodes, spleen, and tumor tissues were surgically removed and dissociated into single-cell suspensions for immune cell analysis. Both the anti-PD-L1 antibody treatment group and the DBE@CCNPs treatment group successfully controlled the growth of tumors in the early stage but rebounded after day 18 (Fig. 4f and S15). It was mainly due to the gradual development of a tumor drug tolerance to the monotherapy. As expected, the tumor growth of the combined treatment group was significantly inhibited, and the tumor inhibition rate was approximately 75% compared with that of the PBS group (Fig. 4g and h). The tumors' H&E slices also showed a higher density of tumor cells in the PBS group, while the tumor cells were significantly eliminated in the treatment group (Fig. S16). The body weights of mice in the combined treatment group did not significantly decrease (Fig. S17), indicating the safety of the combined treatment strategy. Histopathology of the mice main organs and serum biochemical indexes further confirmed this safety as no obvious toxic side effects were observed in mice (Fig. S18–20).

3.6. Antitumor mechanisms of combination therapy

To explore the antitumor mechanisms of the combination therapy, we analyzed the immune cells in the mice lymph nodes and spleens. The results showed that both DBE@CCNPs and combination treatment groups can increase the expression of costimulatory molecules in DCs, while the intraperitoneal injection of an anti-PD-L1 antibody did not significantly stimulate DCs maturation in the lymph nodes (Fig. 5a, b and c). This indicates that the activation of DCs is mainly caused by the activation of Toll-like receptors by immune adjuvants. In addition, the combined treatment group showed the greatest activation effect on DCs in the lymph nodes, and the activation effect was better than that of the DBE@CCNPs group, suggesting that the anti-PD-L1 antibody can enhance the effect of nanovaccine in activating DCs. The proportions of $CD8^+$ T cells in the DBE@CCNPs group and the combination treatment group were significantly increased (Fig. 5d). This was mainly due to the recognition of the DBE@CCNPs nanovaccine by the T cells via the MHC-1-antigen complex and through the cross-presentation of antigens after endocytosis by DCs. These events triggered the activation and proliferation of tumor-specific $CD8^+$ T cells. Besides, if these active T cells were not differentiated into memory T cells, the antitumor immune responses could not achieve long-term effects, and the exhaustion of tumor-specific T cells would also lead to immune resistance [50]. Therefore, we focused on the changes in memory T cells in the spleen. The results demonstrated that the number of central memory $CD8^+$ T cells and their effect in the mice spleen were notably upregulated after combined treatment (Fig. 5e and f). This was probably the main reason why the

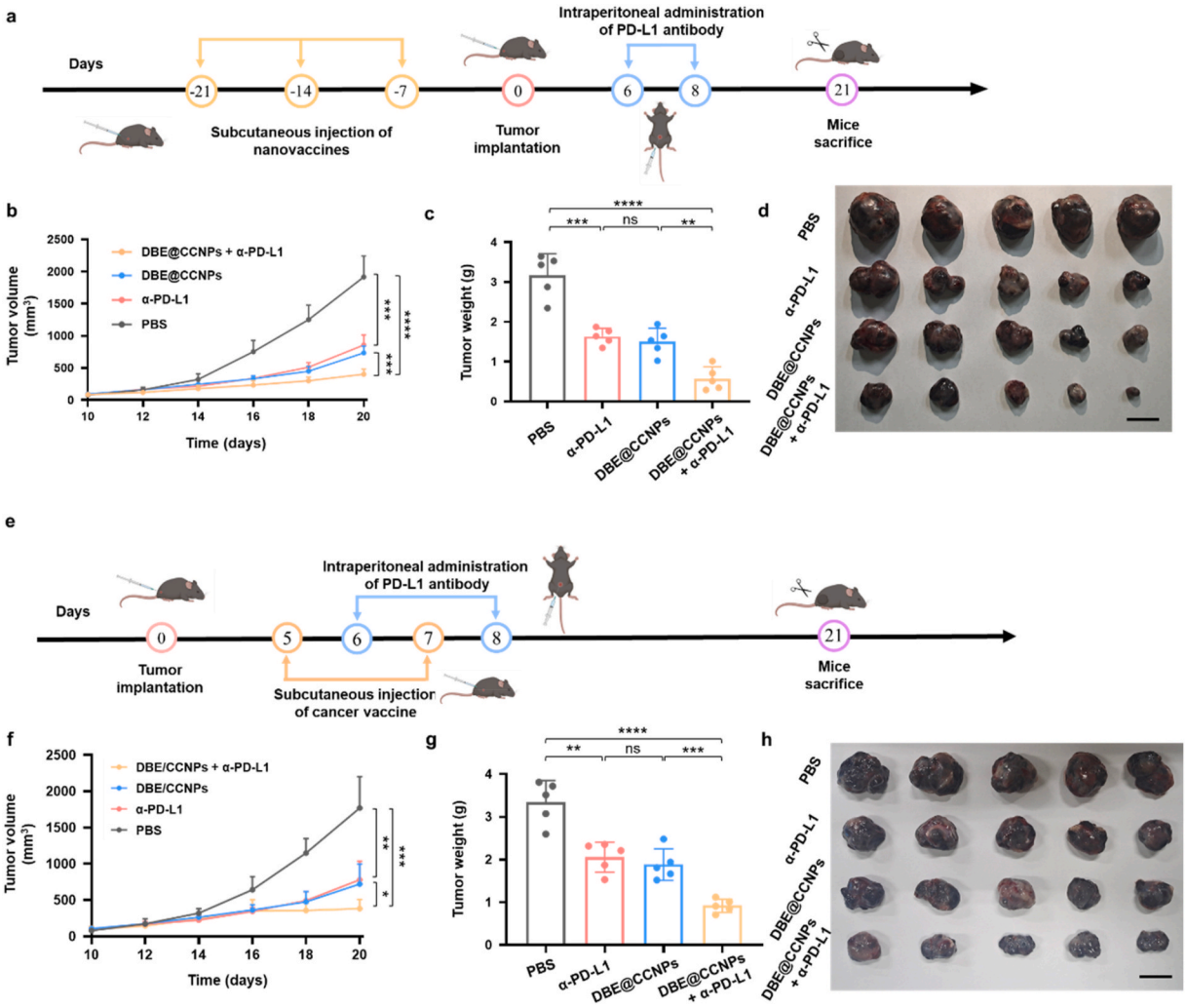

Fig. 4. Nanovaccine combination with a PD-L1 antibody for B16F10 tumor treatment. (a) Schematic illustration of the tumor prevention experiment. (b) Tumor growth curves of different groups. (c) Tumor weights after the preventive experiment. (d) Tumor images after tumor the preventive experiments. Scale bar = 1 cm. (e) Schematic illustration of the tumor treatment experiment. (f) Tumor growth curves of the different groups. (g) Tumor weights after the anti-tumor experiment. (h) Tumor images after the tumor treatment experiments. Scale bar = 1 cm ****p < 0.0001; ***p < 0.001; **p < 0.01; ns, not significant.

tumors in the combined treatment group were well controlled in the later stage of tumor treatment.

Finally, we analyzed the immune cells of the tumors. The results of flow cytometry showed that the number of mature T lymphocytes in the tumor tissue in the combined treatment group significantly increased (Fig. 5g), which could release granzyme and perforin to kill the tumor, indicating that the immune status of the tumor tissues was improved. The results of flow cytometry and IHC showed that both ICB therapy and the tumor nanovaccine can promote the infiltration of $CD8^+$ T cells (Fig. 5h and j). In the combined treatment group, this infiltration was more obvious. Generally, the tumor microenvironment was immunosuppressive, which assisted the immune escape of tumor cells [51,52]. Therefore, we evaluated the activated $CD8^+$ T cells in the tumor microenvironment after treatment. The results showed that the number of activated $CD8^+$ T cells in the tumor microenvironment of the combined treatment group was significantly higher than that in other groups, indicating that the combined therapy reversed the immunosuppressive microenvironment (Fig. 5i). The immunohistochemistry of PD-L1 in tumors showed that the expression of PD-L1 in tumor tissues was upregulated when treated with the tumor nanovaccine (Fig. 5k). This event reduced the activity of infiltrating T cells and impaired the therapeutic effect. When combined with an anti-PD-L1 antibody, PD-L1 was significantly inhibited, and the infiltrating T cells could maintain their antitumor activity and achieve a sustained antitumor effect.

4. Conclusion

In summary, this study designed a dual bioengineering process, which subtly changed the biological signals on the surface of the tumor cell membrane, enhanced the immunogenicity of tumor antigens, and improved the uptake of the nanovaccine by DCs. The nanosized design allows synergistic function between antigens and adjuvants. After subcutaneous injection, the nanovaccine forms an antigen reservoir and activates DCs for a long time. After endocytosis by DCs, the nanovaccine can achieve antigen cross presentation through the process of lysosomal escape, thereby activating a large number of tumor-specific $CD8^+$T cells to kill tumors. In addition, after the combined use of immune checkpoints, the tumor inhibition effect has been further strengthened. This dual bioengineering technology provides a new idea for the development of a personalized tumor vaccine.

Ethical approval

All animal experiments complied with the relevant ethical standards and all procedures were approved by the Animal Care and Use Committee of Yantai University.

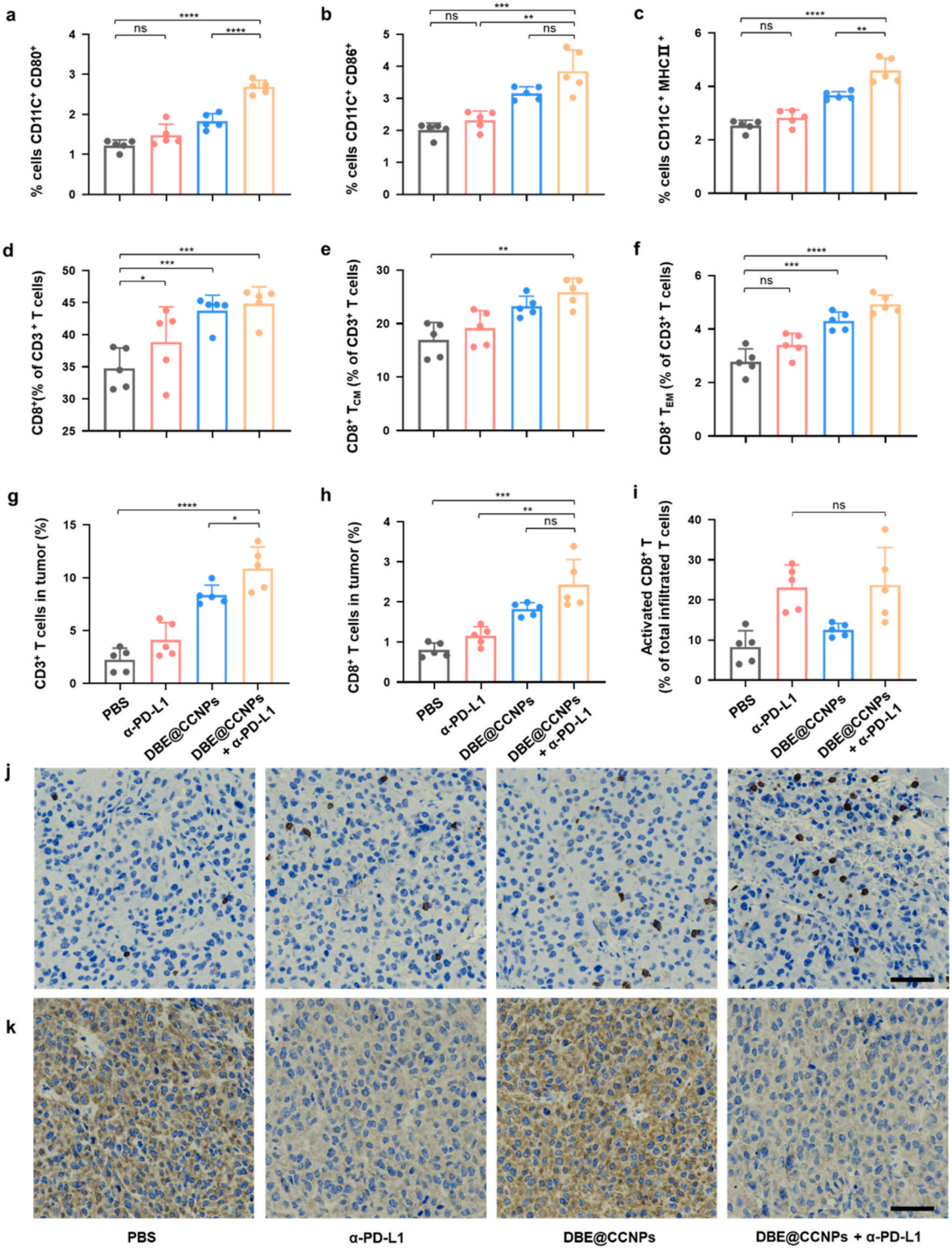

Fig. 5. Combination therapy activates tumor-associated immune cells. Flow cytometry results for (a) $CD11c^+CD80^+$ (b) $CD11c^+$ $CD86^+$ (c) $CD11c^+MHCII^+$ matured DCs of the single cells in TDLNs. Flow cytometry results for (d) $CD8^+$ T cells, (e) $CD8^+$ $CD44^+$ $CD62L^+$ central memory T cells, and (f) $CD8^+CD44^+CD62L^-$ effective memory T cells of the $CD3^+$T cells ratios in spleens. (g) Flow cytometry analyses of $CD45^+CD3^+$T cells ratios in tumors. (h) Flow cytometry analyses of $CD45^+CD3^+CD8^+$T cells ratios in the tumors. (i) Flow cytometry results of $CD69^+$ T cells of total infiltrated T cells in tumors. (j) Immunohistochemical results of tumor-infiltrating T cells. (k) Immunohistochemical results of PD-L1 in tumors. Scale bar = 50 μm ****$p < 0.0001$; ***$p < 0.001$; **$p < 0.01$; *$P < 0.05$; ns, not significant.

CRediT authorship contribution statement

Shengyang Liu: Methodology, Investigation, Experiments, Writing – original draft. **Jiayan Wu:** Experiments, In vitro experiments, Animal experiments, Data curation. **Yuanji Feng:** BMDCs extraction, Animal experiments, Data curation. **Xiaoya Guo:** Animal experiments, Data curation. **Tong Li:** Animal experiments, Data curation. **Meng Meng:** Animal experiments, Data curation. **Jie Chen:** Conceptualization,

Project administration, Writing – review & editing, Funding acquisition. **Daquan Chen:** Resources, Supervision, Funding acquisition. **Huayu Tian:** Conceptualization, Project administration, Funding acquisition, Writing – review & editing.

Declaration of competing interest

The authors declare no competing financial interest.

Acknowledgments

The authors are thankful to the National Key R&D Program of China (2021YFB3800900), National Natural Science Foundation of China (51925305, 51873208, 51973217). Taishan Scholar Foundation of Shandong Province (qnts20161035), Natural Science Foundation of Shandong Province (ZR2019ZD24, ZR2019YQ30), Jilin Province Science and Technology Development Program (20200201075JC, 20210509005RQ).

Appendix A. Supplementary data

Supplementary data to this article can be found online at https://doi.org/10.1016/j.bioactmat.2022.09.017.

References

[1] R.T. Shroff, P. Chalasani, R. Wei, D. Pennington, G. Quirk, M.V. Schoenle, K. L. Peyton, J.L. Uhrlaub, T.J. Ripperger, M. Jergovic, S. Dalgai, A. Wolf, R. Whitmer, H. Hammad, A. Carrier, A.J. Scott, J. Nikolich-Zugich, M. Worobey, R. Sprissler, M. Dake, B.J. LaFleur, D. Bhattacharya, Immune responses to two and three doses of the BNT162b2 mRNA vaccine in adults with solid tumors, Nat. Med. 27 (11) (2021) 2002–2011.

[2] M. Saxena, S.H. van der Burg, C.J.M. Melief, N. Bhardwaj, Therapeutic cancer vaccines, Nat. Rev. Cancer 21 (6) (2021) 360–378.

[3] P.A. Ott, Z. Hu, D.B. Keskin, S.A. Shukla, J. Sun, D.J. Bozym, W. Zhang, A. Luoma, A. Giobbie-Hurder, L. Peter, C. Chen, O. Olive, T.A. Carter, S. Li, D.J. Lieb, T. Eisenhaure, E. Gjini, J. Stevens, W.J. Lane, I. Javeri, K. Nellaiappan, A. M. Salazar, H. Daley, M. Seaman, E.I. Buchbinder, C.H. Yoon, M. Harden, N. Lennon, S. Gabriel, S.J. Rodig, D.H. Barouch, J.C. Aster, G. Getz, K. Wucherpfennig, D. Neuberg, J. Ritz, E.S. Lander, E.F. Fritsch, N. Hacohen, C. J. Wu, An immunogenic personal neoantigen vaccine for patients with melanoma, Nature 547 (7662) (2017) 217–221.

[4] C. Chong, G. Coukos, M. Bassani-Sternberg, Identification of tumor antigens with immunopeptidomics, Nat. Biotechnol. 40 (2) (2022) 175–188.

[5] U. Sahin, Ö. Türeci, Personalized vaccines for cancer immunotherapy, Science 359 (6382) (2018) 1355–1360.

[6] L.M. Sholl, F.R. Hirsch, D. Hwang, J. Botling, F. Lopez-Rios, L. Bubendorf, M. Mino-Kenudson, A.C. Roden, M.B. Beasley, A. Borczuk, E. Brambilla, G. Chen, T.Y. Chou, J.H. Chung, W.A. Cooper, S. Dacic, S. Lantuejoul, D. Jain, D. Lin, Y. Minami, A. Moreira, A.G. Nicholson, M. Noguchi, M. Papotti, G. Pelosi, C. Poleri, N. Rekhtman, M.S. Tsao, E. Thunnissen, W. Travis, Y. Yatabe, A. Yoshida, J. B. Daigneault, A. Zehir, S. Peters, Wistuba II, K.M. Kerr, J.W. Longshore, The promises and challenges of tumor mutation burden as an immunotherapy biomarker: a perspective from the International Association for the Study of Lung Cancer Pathology Committee, J. Thorac. Oncol. 15 (9) (2020) 1409–1424.

[7] L. Ma, L. Diao, Z. Peng, Y. Jia, H. Xie, B. Li, J. Ma, M. Zhang, L. Cheng, D. Ding, X. Zhang, H. Chen, F. Mo, H. Jiang, G. Xu, F. Meng, Z. Zhong, M. Liu, Immunotherapy and prevention of cancer by nanovaccines loaded with whole-cell components of tumor tissues or cells, Adv. Mater. 33 (43) (2021), 2104849.

[8] M.A. Morrissey, N. Kern, R.D. Vale, CD47 ligation repositions the inhibitory receptor SIRPA to suppress integrin activation and phagocytosis, Immunity 53 (2) (2020) 290–302.

[9] P.A. Betancur, B.J. Abraham, Y.Y. Yiu, S.B. Willingham, F. Khameneh, M. Zarnegar, A.H. Kuo, K. McKenna, Y. Kojima, N.J. Leeper, P. Ho, P. Gip, T. Swigut, R. I. Sherwood, M.F. Clarke, G. Somlo, R.A. Young, I.L. Weissman, A CD47-associated super-enhancer links pro-inflammatory signalling to CD47 upregulation in breast cancer, Nat. Commun. 8 (1) (2017), 14802.

[10] A. Veillette, J. Chen, SIRPalpha-CD47 immune checkpoint blockade in anticancer therapy, Trends Immunol. 39 (3) (2018) 173–184.

[11] Y. Li, M. Zhang, X. Wang, W. Liu, H. Wang, Y.G. Yang, Vaccination with CD47 deficient tumor cells elicits an antitumor immune response in mice, Nat. Commun. 11 (1) (2020) 581.

[12] Z. Johnson, A. Papaioannou, L. Bernard, E. Cosimo, B. Daubeuf, F. Richard, X. Chauchet, V. Moine, L. Broyer, L. Shang, M. Deehan, N. Fischer, K. Masternak, M. Kosco-Vilbois, A. Michie, W. Ferlin, Bispecific antibody targeting of CD47/CD19 to promote enhanced phagocytosis of patient B lymphoma cells, J. Clin. Oncol. 33 (15_suppl) (2015) e14016-e14016.

[13] N.J. Lakhani, L.Q.M. Chow, J.F. Gainor, P. LoRusso, K.-W. Lee, H.C. Chung, J. Lee, Y.-J. Bang, F.S. Hodi, W.S. Kim, R. Santana-Davila, P. Fanning, P. Squifflet, F. Jin, T.C. Kuo, H.I. Wan, J. Pons, S.S. Randolph, W.A. Messersmith, Evorpacept alone and in combination with pembrolizumab or trastuzumab in patients with advanced solid tumours (ASPEN-01): a first-in-human, open-label, multicentre, phase 1 dose-escalation and dose-expansion study, Lancet Oncol. 22 (12) (2021) 1740–1751.

[14] B.I. Sikic, N. Lakhani, A. Patnaik, S.A. Shah, S.R. Chandana, D. Rasco, A.D. Colevas, T. O'Rourke, S. Narayanan, K. Papadopoulos, G.A. Fisher, V. Villalobos, S. S. Prohaska, M. Howard, M. Beeram, M.P. Chao, B. Agoram, J.Y. Chen, J. Huang, M. Axt, J. Liu, J.-P. Volkmer, R. Majeti, I.L. Weissman, C.H. Takimoto, D. Supan, H. A. Wakelee, R. Aoki, M.D. Pegram, S.K. Padda, First-in-Human, first-in-class phase I trial of the anti-CD47 antibody Hu5F9-G4 in patients with advanced cancers, J. Clin. Oncol. 37 (12) (2019) 946–953.

[15] M.P. Chao, C.H. Takimoto, D.D. Feng, K. McKenna, P. Gip, J. Liu, J.P. Volkmer, I. L. Weissman, R. Majeti, Therapeutic targeting of the macrophage immune checkpoint CD47 in myeloid malignancies, Front. Oncol. 9 (2019) 1380.

[16] F. Castoldi, E. Vacchelli, L. Zitvogel, M.C. Maiuri, F. Pietrocola, G. Kroemer, Systemic autophagy in the therapeutic response to anthracycline-based chemotherapy, OncoImmunology 8 (1) (2019), e1498285.

[17] J. Fucikova, O. Kepp, L. Kasikova, G. Petroni, T. Yamazaki, P. Liu, L. Zhao, R. Spisek, G. Kroemer, L. Galluzzi, Detection of immunogenic cell death and its relevance for cancer therapy, Cell Death Dis. 11 (11) (2020) 1013.

[18] L. Galluzzi, I. Vitale, S. Warren, S. Adjemian, P. Agostinis, A.B. Martinez, T. A. Chan, G. Coukos, S. Demaria, E. Deutsch, D. Draganov, R.L. Edelson, S. C. Formenti, J. Fucikova, L. Gabriele, U.S. Gaipl, S.R. Gameiro, A.D. Garg, E. Golden, J. Han, K.J. Harrington, A. Hemminki, J.W. Hodge, D.M.S. Hossain, T. Illidge, M. Karin, H.L. Kaufman, O. Kepp, G. Kroemer, J.J. Lasarte, S. Loi, M. T. Lotze, G. Manic, T. Merghoub, A.A. Melcher, K.L. Mossman, F. Prosper, Ø. Rekdal, M. Rescigno, C. Riganti, A. Sistigu, M.J. Smyth, R. Spisek, J. Stagg, B. E. Strauss, D. Tang, K. Tatsuno, S.W. van Gool, P. Vandenabeele, T. Yamazaki, D. Zamarin, L. Zitvogel, A. Cesano, F.M. Marincola, Consensus guidelines for the definition, detection and interpretation of immunogenic cell death, J. Immunother. Cancer 8 (1) (2020), e000337.

[19] L. Galluzzi, A. Buque, O. Kepp, L. Zitvogel, G. Kroemer, Immunogenic cell death in cancer and infectious disease, Nat. Rev. Immunol. 17 (2) (2017) 97–111.

[20] M. Obeid, A. Tesniere, F. Ghiringhelli, G.M. Fimia, L. Apetoh, J.L. Perfettini, M. Castedo, G. Mignot, T. Panaretakis, N. Casares, D. Metivier, N. Larochette, P. van Endert, F. Ciccosanti, M. Piacentini, L. Zitvogel, G. Kroemer, Calreticulin exposure dictates the immunogenicity of cancer cell death, Nat. Med. 13 (1) (2007) 54–61.

[21] Y. Chen, L. Wang, M. Zheng, C. Zhu, G. Wang, Y. Xia, E.J. Blumenthal, W. Mao, Y. Wan, Engineered extracellular vesicles for concurrent Anti-PDL1 immunotherapy and chemotherapy, Bioact. Mater. 9 (2022) 251–265.

[22] H. Fang, Z. Guo, J. Chen, L. Lin, Y. Hu, Y. Li, H. Tian, X. Chen, Combination of epigenetic regulation with gene therapy-mediated immune checkpoint blockade induces anti-tumour effects and immune response in vivo, Nat. Commun. 12 (1) (2021) 6742.

[23] J. Chen, H. Fang, Y. Hu, J. Wu, S. Zhang, Y. Feng, L. Lin, H. Tian, X. Chen, Combining mannose receptor mediated nanovaccines and gene regulated PD-L1 blockade for boosting cancer immunotherapy, Bioact. Mater. 7 (2022) 167–180.

[24] M. Wang, Q. Hu, J. Huang, X. Zhao, S. Shao, F. Zhang, Z. Yao, Y. Ping, T. Liang, Engineered a dual-targeting biomimetic nanomedicine for pancreatic cancer chemoimmunotherapy, J. Nanobiotechnol. 20 (1) (2022) 85.

[25] L. Lin, Y. Hu, Z. Guo, J. Chen, P. Sun, H. Tian, X. Chen, Gene-guided OX40L anchoring to tumor cells for synergetic tumor "self-killing" immunotherapy, Bioact. Mater. (2022).

[26] Y. Hu, L. Lin, J. Chen, K. Hao, S. Zhang, X. Guo, Z. Guo, H. Tian, X. Chen, Highly enhanced antitumor immunity by a three-barreled strategy of the l-arginine-promoted nanovaccine and gene-mediated PD-L1 blockade, ACS Appl. Mater. Interfaces 12 (37) (2020) 41127–41137.

[27] Y. Zhao, Engineering biomimetic epigenetic nanoinducer improves cancer immunotherapy, Sci. China Chem. 64 (12) (2021) 2055–2056.

[28] J. Scheiermann, D.M. Klinman, Clinical evaluation of CpG oligonucleotides as adjuvants for vaccines targeting infectious diseases and cancer, Vaccine 32 (48) (2014) 6377–6389.

[29] Y. Hu, L. Lin, J. Chen, A. Maruyama, H. Tian, X. Chen, Synergistic tumor immunological strategy by combining tumor nanovaccine with gene-mediated extracellular matrix scavenger, Biomaterials 252 (2020), 120114.

[30] R.H. Fang, C.M. Hu, B.T. Luk, W. Gao, J.A. Copp, Y. Tai, D.E. O'Connor, L. Zhang, Cancer cell membrane-coated nanoparticles for anticancer vaccination and drug delivery, Nano Lett. 14 (4) (2014) 2181–2188.

[31] A.V. Kroll, R.H. Fang, Y. Jiang, J. Zhou, X. Wei, C.L. Yu, J. Gao, B.T. Luk, D. Dehaini, W. Gao, L. Zhang, Nanoparticulate delivery of cancer cell membrane elicits multiantigenic antitumor immunity, Adv. Mater. 29 (47) (2017), 1703969.

[32] R. Eil, S.K. Vodnala, D. Clever, C.A. Klebanoff, M. Sukumar, J.H. Pan, D.C. Palmer, A. Gros, T.N. Yamamoto, S.J. Patel, G.C. Guittard, Z. Yu, V. Carbonaro, K. Okkenhaug, D.S. Schrump, W.M. Linehan, R. Roychoudhuri, N.P. Restifo, Ionic immune suppression within the tumour microenvironment limits T cell effector function, Nature 537 (7621) (2016) 539–543.

[33] J. Qi, F. Jin, Y. You, Y. Du, D. Liu, X. Xu, J. Wang, L. Zhu, M. Chen, G. Shu, L. Wu, J. Ji, Y. Du, Synergistic effect of tumor chemo-immunotherapy induced by leukocyte-hitchhiking thermal-sensitive micelles, Nat. Commun. 12 (1) (2021) 4755.

[34] G. Hasko, J. Linden, B. Cronstein, P. Pacher, Adenosine receptors: therapeutic aspects for inflammatory and immune diseases, Nat. Rev. Drug Discov. 7 (9) (2008) 759–770.

[35] A. Young, S.F. Ngiow, Y. Gao, A.M. Patch, D.S. Barkauskas, M. Messaoudene, G. Lin, J.D. Coudert, K.A. Stannard, L. Zitvogel, M.A. Degli-Esposti, E. Vivier, N. Waddell, J. Linden, N.D. Huntington, F. Souza-Fonseca-Guimaraes, M.J. Smyth, A2AR adenosine signaling suppresses natural killer cell maturation in the tumor microenvironment, Cancer Res. 78 (4) (2018) 1003–1016.

[36] S.K. Vodnala, R. Eil, R.J. Kishton, M. Sukumar, T.N. Yamamoto, N.H. Ha, P.H. Lee, M. Shin, S.J. Patel, Z. Yu, D.C. Palmer, M.J. Kruhlak, X. Liu, J.W. Locasale, J. Huang, R. Roychoudhuri, T. Finkel, C.A. Klebanoff, N.P. Restifo, T cell stemness and dysfunction in tumors are triggered by a common mechanism, Science 363 (6434) (2019) eaau0135.

[37] D. Wang, S. Wang, Z. Zhou, D. Bai, Q. Zhang, X. Ai, W. Gao, L. Zhang, White blood cell membrane-coated nanoparticles: recent development and medical applications, Adv. Healthc. Mater. 11 (7) (2022), 2101349.

[38] J. Wang, S. Wang, T. Ye, F. Li, X. Gao, Y. Wang, P. Ye, S. Qing, C. Wang, H. Yue, J. Wu, W. Wei, G. Ma, Choice of nanovaccine delivery mode has profound impacts on the intralymph node spatiotemporal distribution and immunotherapy efficacy, Adv. Sci. 7 (19) (2020), 2001108.

[39] J.R. Ohlfest, B.M. Andersen, A.J. Litterman, J. Xia, C.A. Pennell, L.E. Swier, A. M. Salazar, M.R. Olin, Vaccine injection site matters: qualitative and quantitative defects in CD8 T cells primed as a function of proximity to the tumor in a murine glioma model, J. Immunol. 190 (2) (2013) 613–620.

[40] Z. Guo, L.J. Kubiatowicz, R.H. Fang, L. Zhang, Nanotoxoids: biomimetic nanoparticle vaccines against infections, Adv. Ther. 4 (8) (2021), 2100072.

[41] J.H. Park, Y. Jiang, J. Zhou, H. Gong, A. Mohapatra, J. Heo, W. Gao, R.H. Fang, L. Zhang, Genetically engineered cell membrane–coated nanoparticles for targeted delivery of dexamethasone to inflamed lungs, Sci. Adv. 7 (25) (2021), eabf7820.

[42] H. Fang, L. Lin, J. Chen, J. Wu, H. Tian, X. Chen, Zinc ion coordination significantly improved the transfection efficiency of low molecular weight polyethylenimine, Biomater. Sci. 7 (4) (2019) 1716–1728.

[43] L. Zhao, Y. Li, D. Pei, Q. Huang, H. Zhang, Z. Yang, F. Li, T. Shi, Glycopolymers/PEI complexes as serum-tolerant vectors for enhanced gene delivery to hepatocytes, Carbohydr. Polym. 205 (2019) 167–175.

[44] A.W. Orr, C.E. Pedraza, M.A. Pallero, C.A. Elzie, S. Goicoechea, D.K. Strickland, J. E. Murphy-Ullrich, Low density lipoprotein receptor–related protein is a calreticulin coreceptor that signals focal adhesion disassembly, J. Cell Biol. 161 (6) (2003) 1179–1189.

[45] X. Hong, X. Zhong, G. Du, Y. Hou, Y. Zhang, Z. Zhang, T. Gong, L. Zhang, X. Sun, The pore size of mesoporous silica nanoparticles regulates their antigen delivery efficiency, Sci. Adv. 6 (25) (2020) eaaz4462.

[46] S. Jung, J. Kim, S. Pramanick, H. Park, H. Lee, J. Lee, W.J. Kim, A Pt(iv)-mediated polymer architecture for facile and stimuli-responsive intracellular gene silencing with chemotherapy, Biomater. Sci. 6 (12) (2018) 3345–3355.

[47] A. Garcia-Diaz, D.S. Shin, B.H. Moreno, J. Saco, H. Escuin-Ordinas, G.A. Rodriguez, J.M. Zaretsky, L. Sun, W. Hugo, X. Wang, G. Parisi, C.P. Saus, D.Y. Torrejon, T. G. Graeber, B. Comin-Anduix, S. Hu-Lieskovan, R. Damoiseaux, R.S. Lo, A. Ribas, Interferon receptor signaling pathways regulating PD-L1 and PD-L2 expression, Cell Rep. 29 (11) (2019) 3766.

[48] Y. Hu, L. Lin, Z. Guo, J. Chen, A. Maruyama, H. Tian, X. Chen, In situ vaccination and gene-mediated PD-L1 blockade for enhanced tumor immunotherapy, Chin, Chem. Lett. 32 (5) (2021) 1770–1774.

[49] A. Ribas, Adaptive immune resistance: how cancer protects from immune attack, Cancer Discov. 5 (9) (2015) 915–919.

[50] Q. Lei, D. Wang, K. Sun, L. Wang, Y. Zhang, Resistance mechanisms of anti-PD1/PDL1 therapy in solid tumors, Front. Cell Dev. Biol. 8 (2020) 672.

[51] M. Binnewies, E.W. Roberts, K. Kersten, V. Chan, D.F. Fearon, M. Merad, L. M. Coussens, D.I. Gabrilovich, S. Ostrand-Rosenberg, C.C. Hedrick, R. H. Vonderheide, M.J. Pittet, R.K. Jain, W. Zou, T.K. Howcroft, E.C. Woodhouse, R. A. Weinberg, M.F. Krummel, Understanding the tumor immune microenvironment (TIME) for effective therapy, Nat. Med. 24 (5) (2018) 541–550.

[52] X. Wang, L.P. Hu, W.T. Qin, Q. Yang, D.Y. Chen, Q. Li, K.X. Zhou, P.Q. Huang, C. J. Xu, J. Li, L.L. Yao, Y.H. Wang, G.A. Tian, J.Y. Yang, M.W. Yang, D.J. Liu, Y. W. Sun, S.H. Jiang, X.L. Zhang, Z.G. Zhang, Identification of a subset of immunosuppressive P2RX1-negative neutrophils in pancreatic cancer liver metastasis, Nat. Commun. 12 (1) (2021) 174.